Available online at www.sciencedirect.com
SCIENCE DIRECT®
ELSEVIER
Journal of Crystal Growth 251 (2003) 118–123
JOURNAL OF CRYSTAL GROWTH
www.elsevier.com/locate/jcrysgro

Effects of noise level in fitting in situ optical reflectance spectroscopy data ☆

Chihchiang Fu*, K.A. Bertness, C.M. Wang

National Institute of Standards and Technology, Optoelectronics Institute, 325 Broadway, Boulder, CO 80305, USA

Abstract

Curve fitting of simulated optical reflectance spectroscopy data is used to evaluate the accuracy of parameters derived from the fits of actual data. These simulations show that to determine the index of refraction n to an accuracy of 0.0015 (corresponding 0.044% for $Al_{0.5}Ga_{0.5}As$ at growth temperature), a reflectance noise with standard deviation $\sigma \leqslant 0.00005$ is required if the absolute reflectance calibration is unknown. The simulations also show that when the absolute reflectance is known within $\pm 0.05\%$, a noise of up to $\sigma = 0.0008$ would result in the same desired accuracy for n. The factors contributing to the uncertainty of the reflectance scaling factor include the temperatures of the photodetectors, stability of light intensity, and deposits on the window of the growth chamber. These factors are investigated experimentally and possible solutions that will allow calibration within the goal range are discussed.

PACS: 81.05.Ea; 81.15.Hi; 81.70.Jb

Keywords: A1. Characterization; A3. Molecular beam epitaxy; B2. Semiconducting aluminum compounds; B2. Semiconducting gallium compounds

1. Introduction

Parameters such as the growth rate and the index of refraction of growing films can be extracted from in situ optical reflectance spectroscopy (ORS) data. These parameters must be accurate to be useful in providing real-time feedback in epitaxial crystal growth [1–6]. A typical goal is to determine the composition of $Al_xGa_{1-x}As$ to $x = \pm 0.002$. The film composition is extracted from the index of refraction n of the film, one of the parameters in the nonlinear fit of a curve to the in situ ORS data. The accuracy of the fitting result is determined by such factors as the noise level of ORS data and the uncertainty in the absolute calibration of the magnitude of the reflectance. This uncertainty is represented by an overall scaling factor in modeling the reflectance with the virtual interface model [2]. Simulated ORS data curves with known parameters and added noise were generated and fit to determine the combinations of noise and scaling factor that will give acceptable results. The simulation results show that a scaling factor known within $\pm 0.05\%$ will meet the composition accuracy goal of ± 0.002, or an index of refraction n accurate to

☆This paper is a contribution of an agency of the U.S. government and is not subject to copyright.

*Corresponding author. Tel.: +1-303-497-5572; fax: +1-303-497-3387.

E-mail address: cfu@boulder.nist.gov (C. Fu).

0022-0248/03/$ - see front matter © 2002 Elsevier Science B.V. All rights reserved.
doi:10.1016/S0022-0248(02)02282-0

0.0015. To achieve this scaling factor range, several factors must be monitored or controlled. These factors include the drift in photodetector temperatures, stability of the ORS light source, and transparency changes of the window of the growth chamber. Each of these factors may also depend on wavelength. We have evaluated these factors for our system, and we discuss the best way to obtain the narrowest range of scaling factor.

2. Experimental procedure

The sensitivity of the ORS data fits to noise level and drift were evaluated by fitting curves of simulated reflectance as a function of time. A conventional thin-film reflectance model [7] was used to generate the curves, and Gaussian noise was added. For this study we simulated the growth of $Al_{0.5}Ga_{0.5}As$ on GaAs at 600°C, with a film index of refraction of 3.400 monitored at a wavelength of 925 nm. The uncertainty in the absolute calibration of the magnitude of the reflectance is represented by an uncertainty in an overall scaling factor applied to the reflectance as part of the fitting process. The uncertainty range of the scaling factor is used as a constraint in the curve-fitting procedure. The simulated data curves were then fit by means of a nonlinear Levenberg–Marquardt algorithm. Fitting results for different noise levels were compared to the known parameters that were used to generate the ORS curves. To assess the overall accuracy of the parameters derived from the simulated data, the curves were divided into sections of 600 s, which were fit individually. Sections of longer time can give better accuracy in terms of matching the known parameters, but they are not as useful in monitoring growth, where the goal is to monitor how conditions are changing in time. Fig. 1 is a section of a generated ORS data curve with added Gaussian noise of $\sigma = 0.0008$ along with the fitted curve and the residuals (difference between simulated data and fit). Curves with different realizations of noise having the same standard deviation were also fit.

The ORS experiment setup is similar to that in Ref. [8]. Briefly, light is generated by a 100 W quartz–tungsten–halogen (QTH) lamp, chopped at a frequency of 325 Hz, and passed through a monochromator. The light is taken from the output of the monochromator through an optical fiber to a small optical breadboard mounted on a window of the molecular beam epitaxy (MBE) chamber. This window is located about 65 cm from the substrate and allows the incoming and

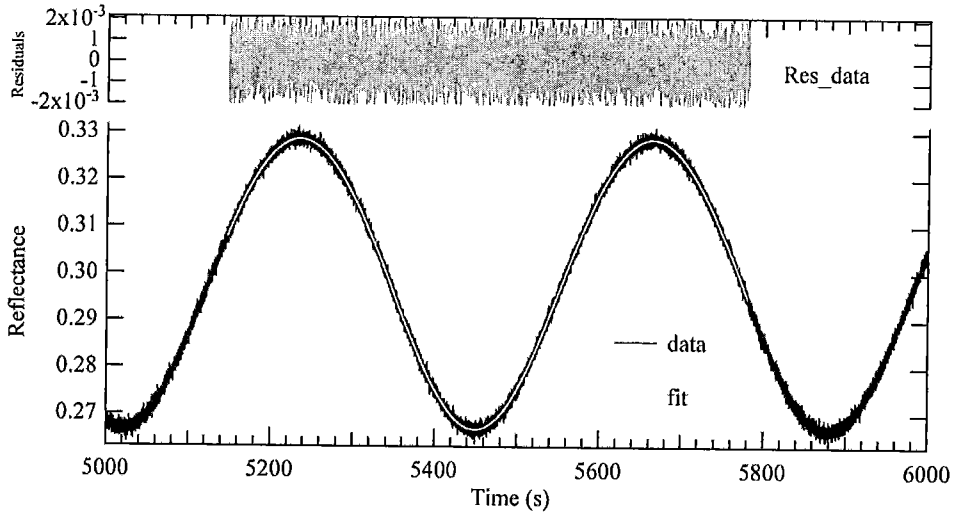

Fig. 1. One section of a generated ORS data curve (data) at wavelength 925 nm from an AlGaAs layer with index of refraction of 3.400 and added Gaussian noise of $\sigma = 0.0008$. The fitted curve is represented by "fit" in the figure. The residuals of the generated data curve (data) and fitted curve (fit) are also plotted.

outgoing reflectance beams to be at near-normal incidence to the substrate. The window is heated to reduce deposition on the inner surface of the window during growth. A beam splitter directs approximately half of the light from the monochromator via the fiber into a reference detector on the optical breadboard. The power source of the QTH lamp is a radiometric power supply that was operated either in constant-current mode or constant-power mode. The photodetectors for both signal and reference are Si photodetectors with built-in amplifiers. There are, in all, three stages of amplification for the detector signals: the built-in amplifier of the photodetector, a voltage pre-amplifier, and a lock-in amplifier. The voltage pre-amplifiers are set to high pass with a cut-off frequency of 100 Hz to reduce sensitivity to 60 Hz noise. The signal lock-in amplifier is set to a time constant of 50 ms to enable sufficient time resolution and average some noise.

To investigate practical limits to noise and scaling factor drift, in situ reflectance data were acquired from a mirror specimen. This specimen was a silicon wafer coated with standard Al and MgF_2 layers, and its reflectance was measured ex situ with a calibrated spectrophotometer. It was loaded into the MBE growth chamber and heated to about 200°C to prevent As deposits. The signal and reference photodetectors in this ORS experiment are equipped with precision thermistors that can measure temperature to 0.01°C resolution. The probe tips of those thermistors are located next to the photodiode cans, and temperatures are monitored simultaneously with both reference and signal data.

3. Results

Curve-fitting results of simulated data with different noise levels show that the accuracy of curve fitting depends on noise level and on the uncertainty range of the scaling factor. Fig. 2 shows the results for fitting without constraints on the overall scaling factor, i.e., when the absolute calibration of the reflectance is not well known. The maximum and minimum values of the parameters (represented as error bars in Figs. 2 and 3) produced in the resulting fits are used as a measure of the uncertainty in refraction index. Under these conditions, a noise level of $\sigma = 0.00005$, or 0.017% for reflectance of 0.3, is needed

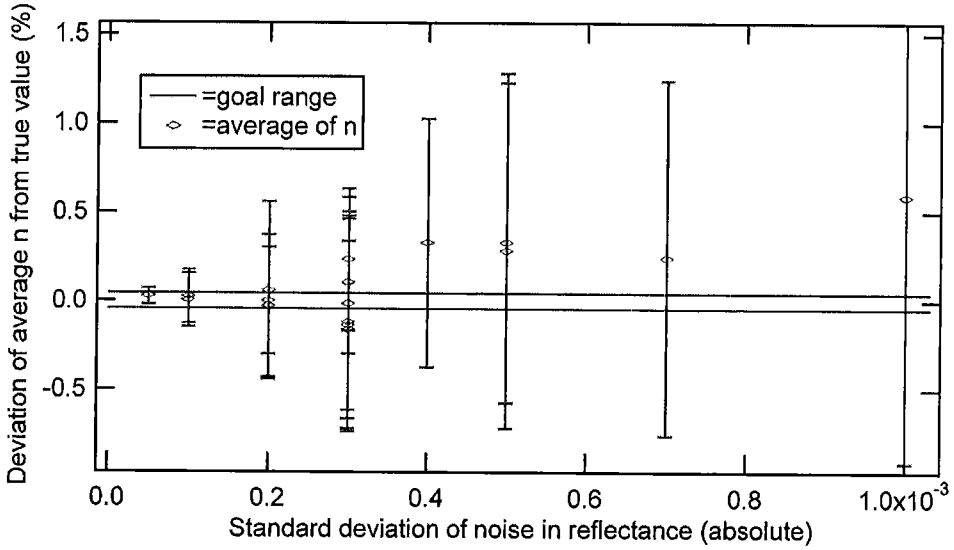

Fig. 2. Deviation of average index of refraction n at wavelength 925 nm from the true value when the scaling factor error is unconstrained. The error bars represent the distribution range of fits to individual realizations of simulated data. The average index of refraction starts to drift away from the true value when the standard deviation of the noise level is higher than $\sigma = 0.0003$. The horizontal solid lines represent the goal.

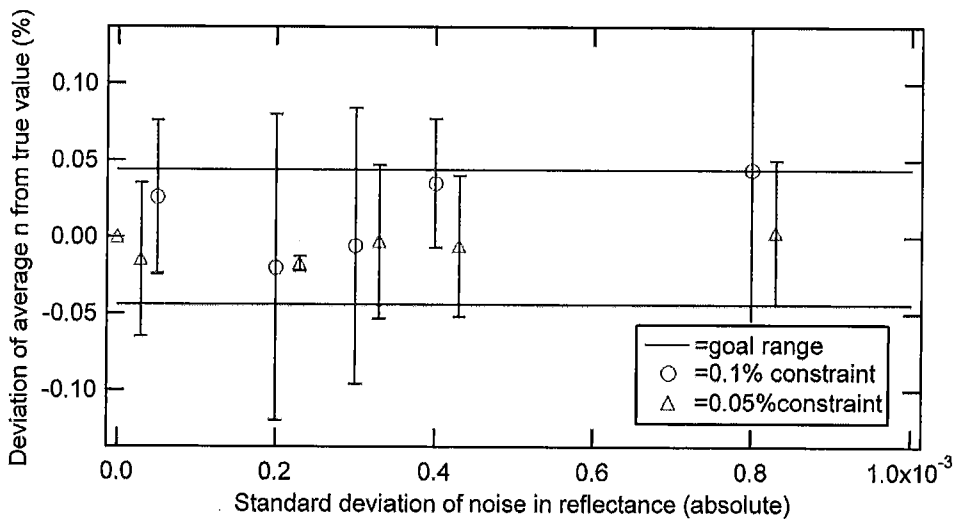

Fig. 3. Deviation of average index of refraction n at wavelength 925 nm from the true value when scaling factor is known within $\pm 0.1\%$ (circles) and $\pm 0.05\%$ (triangles, shifted slightly to the right for clarity). When the scaling factor is known within $\pm 0.05\%$, a reflectance noise level up to $\sigma = 0.0008$ can be tolerated for average reflectance of 0.3.

to achieve the index accuracy goal of 0.0015. Fig. 3 shows the relation between the accuracy of the index of refraction and noise level when the scaling factor error is constrained to a small range about its known value. When ORS data were fit with a constraint of $\pm 0.05\%$ on the scaling factor, noise levels in reflectance up to a $\sigma = 0.0008$, or 0.27% for average reflectance of 0.3, can be tolerated.

A reflectance noise level of $\sigma = 0.00005$ is not achievable in practice. However, it is relatively easy to achieve the experimental noise level needed to meet the composition accuracy goal when the scaling factor is known to 0.05%. For the mirror sample, the maximum noise level that can be tolerated is $\sigma = 0.0023$, or 0.27% at 925 nm. To minimize the noise levels, different gain combinations of the three amplification stages were compared. Noise levels with all three stages of amplification in operation are similar. The noise level increased if any one of the three stages of amplification was omitted. Typical noise levels are 0.21% (standard deviation $\sigma = 0.00166$ for reflectance of 0.8045 at 850 nm), 0.091% ($\sigma = 0.00078$) at 925 nm, and 0.086% ($\sigma = 0.00079$) at 1050 nm. The primary advantage of using the detectors with built-in pre-amplification is being able to move to higher frequency. External current pre-amplifiers did not have adequate bandwidth to operate above 300 Hz at the high gain needed to boost the signal above background electromagnetic noise.

One significant source of calibration drift is the temperature dependence of the photodiode sensitivity. According to the manufacturer's data, the temperature dependence of the photodiode sensitivity varies with wavelength. To investigate this temperature effect at different wavelengths, the temperature and signal level of both the signal and reference detectors were measured in the range 25–32°C, which is the typical temperature change for the reference detector during a day. There is some inaccuracy in the temperature measurement caused by heat transfer through the lead of the probe and by time lags while the temperature of the detector case equilibrates. Ref. [9] suggests that it is sufficient to use a linear approximation for the temperature dependence and to express the temperature dependence as a percent change in signal per degree; therefore, the percent change per degree was calculated using the photodiode signal vs. temperature plot.

Since the light intensity is not perfectly constant in time, the voltage variations of the reference detector include effects of both temperature and light intensity. In order to separate these effects,

the change of light intensity must be compensated. First, the rate of variation of light intensity was calculated from a data region where the detector temperature change was small (less than 1°C). This voltage change per second was subtracted from data where the temperature change was substantial in order to calculate a temperature sensitivity coefficient. Fig. 4 shows the detector voltage percent change per degree Celsius after the change in light intensity with time had been compensated. The vertical uncertainty bars were calculated assuming that the rate of change of light intensity varies up to ±50%. At 1050 nm, the detector has the largest relative change per degree Celsius change, averaging 1.0%/°C. The experiment also shows that the detector's sensitivity to temperature is much lower at 850 and 925 nm compared to measurements at 1050 nm.

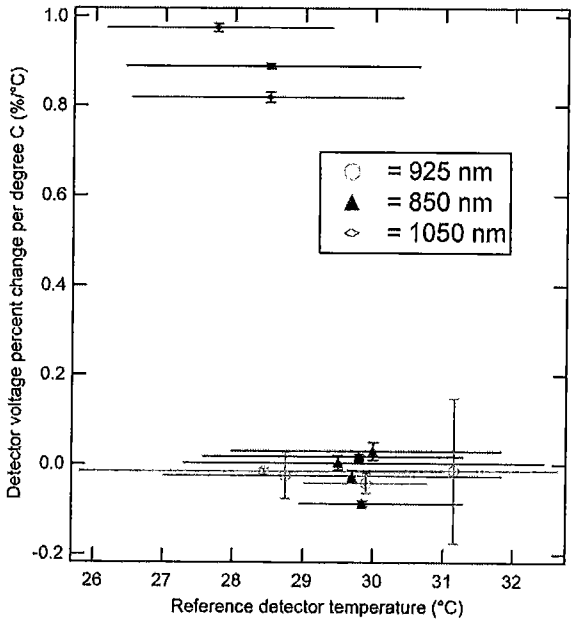

Fig. 4. Change of reference detector voltage with temperature at different wavelengths. The error bars represent the uncertainty in the intensity compensation. The horizontal lines represent the temperature range of the data used to calculate the slope.

Even when temperature drifts are taken into account, there is some residual drift in the calibration of the absolute reflectance. Signal-to-reference ratios at 925, 850, and 1050 nm for the mirror sample were taken on different days and at different times of each day to evaluate the stability of the ratio. The values have been normalized to the average ratio at each wavelength and are plotted in Fig. 5. As can be seen, even after correcting for temperature drift in the photodetectors, there is still a great deal of variation in the calibration over time. At 850 and 925 nm, the uncertainty (2σ) in calibration over 4 days is 0.5%,

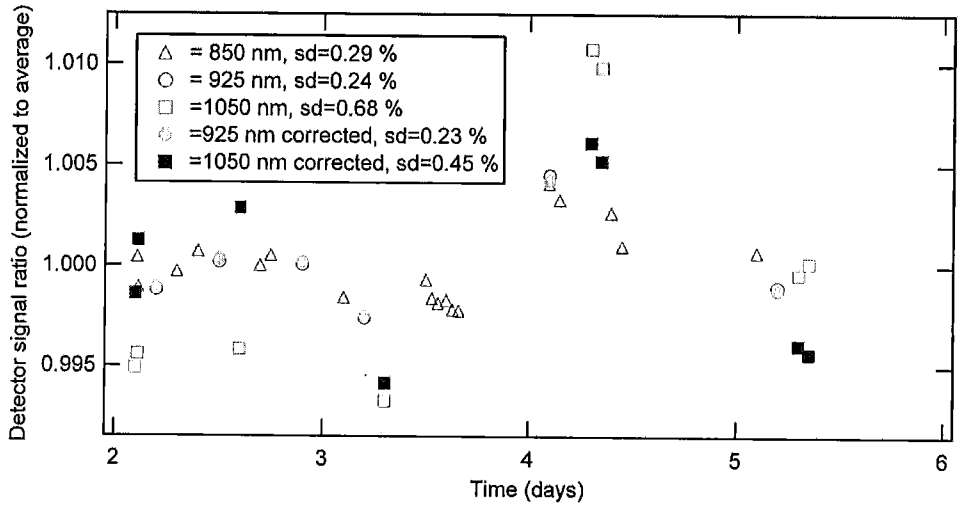

Fig. 5. Signal-to-reference ratios of photodetector signals for the reference mirror specimen at different times over a 4-day range. Three different wavelengths, 1050 nm (squares), 925 nm (circles), and 850 nm (triangles), are shown. The data sets for each wavelength are normalized to their average value, and the standard deviations (sd) of the distributions are given in the legend.

Table 1
Window transmission normalized to the value at the center of the window for different wavelengths and window locations

	600 nm	925 nm	1000 nm
Center of window	1.0000	1.0000	1.0000
Upper right	1.0058	1.0004	1.0012
Upper left	1.0992	1.0154	1.0141
Left	1.0450	1.0143	1.0127
Lower left	1.1493	1.0443	1.0368
Lower right	1.1084	1.0042	0.9980

or approximately 10 times the goal needed for determination of composition within 0.002 in Al mole fraction. The source of the remaining drift has not yet been identified. One possibility is that over time there are changes in window transmittance due either to temperature changes in the window or to changes in deposit thickness and other imperfections on the window. Table 1 shows the wavelength dependence of the window transmittance. The increase in absorption at shorter wavelengths suggests that the thin coating that builds up in time may be amorphous GaAs. The beam may also drift spatially, causing the efficiency (e.g., reflectance, transmittance, detector responsivity) of the various optical components to vary.

4. Conclusion

In order to determine how to increase the accuracy of the parameters extracted from in situ ORS data, simulated data curves with added noise were analyzed with nonlinear regressive curve fitting. A combination of a practically achievable noise level of $\sigma < 0.0008$ and an absolute calibration accuracy (scaling factor) within $\pm 0.05\%$ was found to allow determination of index of refraction sufficiently accurate to determine the Al mole fraction of AlGaAs films to within 0.002. Achieving this noise specification in actual experimental conditions was possible, but the drift in the reflectance calibration exceeds the scaling factor specification for times greater than approximately 1 day. Part of the drift is attributed to the photodetectors, which were found to significantly dependent on temperature at 1050 nm, with much smaller dependence at 925 and 850 nm. Nonuniformity of window deposits and spatial variations in the optical efficiency of the various optical components are believed to be responsible for the remaining drift. These results suggest that it will be difficult to measure film composition accurately using values of index of refraction derived from ORS unless the system is calibrated frequently.

References

[1] K.A. Bertness, R.K. Hickernell, S.P. Hays, D.H. Christensen, J. Vac. Sci. Technol. B 16 (3) (1998) 1.
[2] D.E. Aspnes, R. Bhat, et al., J. Crystal Growth 120 (1–4) (1992) 71.
[3] Y.M. Houng, M.R.T. Tan, B.W. Liang, S.Y. Wang, D.E. Mars, J. Vac. Sci. Technol. B 12 (2) (1994) 1221.
[4] P. Kurpas, A. Rumberg, M. Weyers, K. Knorr, T. Bergunde, M. Sato, W. Richter, J. Crystal Growth 170 (1–4) (1997) 203.
[5] T. Makimoto, Y. Yamauchi, N. Kobayashi, Y. Horikoshi, Jpn. J. Appl. Phys. 29 (1990) L207.
[6] W.T. Taferner, D.L. Dorsey, K. Mahalingham, K.G. Eyink, Real-time monitoring by spectroscopic ellipsometry and desorption mass spectroscopy during molecular beam epitaxy of AlGaAs/GaAs at high substrate temperatures, Materials Research Society Symposium Proceedings, Vol. 569, MRS, Pittsburgh, 1999, pp. 107–112.
[7] W.G. Breiland, K.P. Kileen, J. Appl. Phys. 78 (11) (1995) 6726.
[8] K.A. Bertness, J. Vac. Sci. Technol. B 18 (3) (2000) 1426.
[9] G. Eppeldauer, Temperature monitored/controlled silicon photodiodes for standardization, SPIE, Surveillance Technologies, Vol. 1479, 1991, pp. 71–77.